

Preparation of three-dimensional macroporous–mesoporous lithium ion sieve with high Li⁺ adsorption capacity

Na Li¹ · Kaifeng Gan¹ · Deli Lu² · Jinlong Zhang¹ · Lingzhi Wang¹

Received: 11 August 2017 / Accepted: 22 September 2017 / Published online: 4 October 2017
© Springer Science+Business Media B.V. 2017

Abstract A three-dimensionally macroporous–mesoporous lithium ion sieve (3DM-H₄Ti₅O₁₂) was transformed from 3DM-Li₄Ti₅O₁₂ through washing with HCl solution, which was synthesized by a combination of hydrothermal and low-temperature calcination (600 °C) treatment, using polystyrene microarray as hard-template, and titanium isopropoxide and lithium acetate as co-precursors. The influence of HCl concentration and temperature on the deintercalation rate of Li and Ti from Li₄Ti₅O₁₂ was specifically explored to maximize the extraction ratio of Li/Ti. The acceleration of Li extraction and insertion in a porous structure was verified using nonporous Li₄Ti₅O₁₂ as a control. 3DM-H₄Ti₅O₁₂ showed superior Li⁺ adsorption performance (5.51 mmol/g) compared with its nonporous counterpart (1.12 mmol/g), which was ascribed to the reduced Li⁺ mass transfer resistance in the highly interconnected porous channel. The ion selectivity of the 3DM-H₄Ti₅O₁₂ lithium ion sieve followed the order of Li⁺ > Na⁺ ~ Ca²⁺ > K⁺ > Mg²⁺. The adsorption performance could be maintained after six cycles. The high adsorption capacity, excellent selectivity, and good recyclability demonstrate the prosperous potential application of 3DM-H₄Ti₅O₁₂.

Na Li and Kaifeng Gan have contributed equally to this paper.

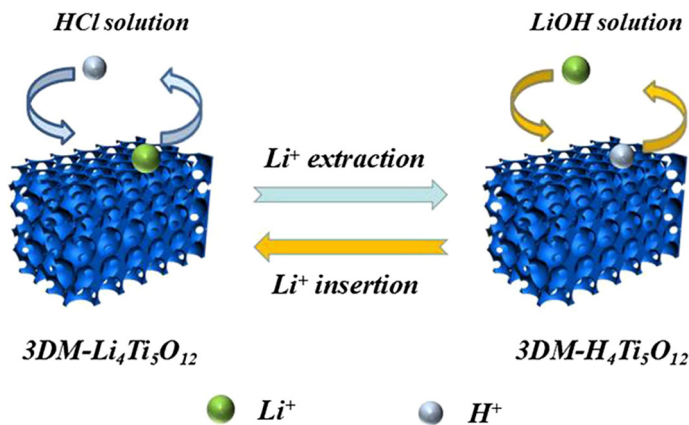
✉ Jinlong Zhang
jlzhang@ecust.edu.cn

✉ Lingzhi Wang
wlz@ecust.edu.cn

¹ Key Laboratory for Advanced Materials and Institute of Fine Chemicals, East China University of Science and Technology, Shanghai 200237, People's Republic of China

² School of Chemical and Environmental Engineering, Shanghai Institute of Technology, Shanghai 201418, People's Republic of China

Graphical Abstract



Keywords 3D · Macroporous · Lithium ion sieve · $Li_4Ti_5O_{12}$

Introduction

Lithium as a new type of energy metal is widely applied in lithium ion batteries [1], the metal smelting, aircraft, and nuclear industries [2–4]. The world demand for lithium is growing rapidly every year, imposing great pressures on lithium production. At present, metal lithium mainly derives from lithium ore, which is, however, falling behind the increasing market demand and suffers from shortcomings including high energy consumption, strict equipment requirements and low recovery rate. Lithium resources in salt lakes account for 69% of the world’s lithium reserves [5, 6], which is expected to be able to supply sufficient lithium. Currently, technologies including solvent extraction [7], ion exchange [8], precipitation [9], and nanofiltration [10] have been applied to obtain lithium from brine. However, a friendly and energy-saving method which can efficiently separate lithium from other metal ions in salt-lake brines still remains a great challenge.

In recent years, the lithium ion sieve [11] has gained wide interest because of its excellent selectivity towards lithium ion. It is prepared by first forming a highly crystallized lithium compound, then generating lithium vacancies with “volume effects” through acid treatment. This kind of memory ability of lithium vacancies makes the lithium ion sieve competent to selectively adsorb and enrich lithium ions [12]. Manganese oxide ($Li_4Mn_5O_{12}$, $LiMn_2O_4$, $Li_{1.6}Mn_{1.6}O_4$, MnO_2) [13–16] and titanium oxide (Li_2TiO_3 , $Li_4Ti_5O_{12}$) [17] are most commonly used precursors for the lithium ion sieve. For example, Shi et al. adopted spinel manganese oxide foam as a lithium ion adsorbent, which was prepared from a polyurethane template and treated with HCl solution to extract the lithium. This kind of material exhibited considerable Li^+ adsorption capacities of 8.73, 3.83 and 1.49 mg/g in LiOH

solution, LiCl buffer solution and lithium-enriched salt lake brine, respectively [18]. Yu et al. synthesized Li_2TiO_3 ternary oxide precursors via a simple solid-phase reaction between Li_2CO_3 and TiO_2 . After the acid treatment, the adsorption of the lithium ion sieve was up to 6.88 mg/g [19]. Compared with its manganese-type counterpart, a titanium-based ion sieve is more chemically stable due to the stronger Ti–O bond [20]. However, research on a titanium-based ion sieve has long been restricted by poor control of the hydrolysis of the titanium precursor. It is still challenging to synthesize an efficient titanium-based lithium ion sieve with high specific surface area and lower mass transfer resistance.

Here, a macroporous–mesoporous lithium titanate ($\text{Li}_4\text{Ti}_5\text{O}_{12}$) with inverse opal structure was synthesized using a closely packed PS microarray as the hard template, where titanium isopropoxide and lithium acetate as the precursors were soaked into the void of the microarray and in situ hydrothermally crystallized, and the PS template was finally removed through calcination. The influence of calcination time and temperature on the crystallite phase and crystallinity of the product was specifically explored. 3DM- $\text{H}_4\text{Ti}_5\text{O}_{12}$ was formed through HCl washing and applied as the lithium ion sieve, which showed improved adsorption capacity towards lithium ions compared with the nonporous $\text{H}_4\text{Ti}_5\text{O}_{12}$ counterpart.

Experimental

Materials

Styrene (C_8H_8 , AR) and magnesium chloride hexahydrate ($\text{MgCl}_2 \cdot 6\text{H}_2\text{O}$, 98.0%, AR) were purchased from Sinopharm Chemical Reagent (Shanghai China). Anhydrous ethanol (EtOH, $\geq 99.7\%$, AR), sodium chloride (NaCl, 99.5%, AR) and ammonia chloride (NH_4Cl , $\geq 98.0\%$, AR) were purchased from Shanghai Titan Scientific (Shanghai, China). Other reagents including potassium persulfate ($\text{K}_2\text{S}_2\text{O}_8$, 99.5%, AR), sodium dodecyl sulfate (SDS, AR), titanium isopropoxide ($\text{C}_{12}\text{H}_{28}\text{O}_4\text{Ti}$, 95%, AR), acetic acid (CH_3COOH , AR), isopropanol ($i\text{-C}_3\text{H}_7\text{OH}$, $\geq 99.7\%$, AR), hydrochloric acid (HCl, 36–38%, AR), ammonium hydroxide ($\text{NH}_3 \cdot \text{H}_2\text{O}$, 25–28%, AR), potassium chloride (KCl, $\geq 99.5\%$, AR) and calcium chloride anhydrous (CaCl_2 , $\geq 96.0\%$, AR) were purchased from Shanghai LingFeng Reagent (Shanghai, China). Lithium acetate (CH_3COOLi , 99.99%, AR), lithium acetate dihydrate ($\text{CH}_3\text{COOLi} \cdot 2\text{H}_2\text{O}$, 99.99%, AR), poly (ethylene glycol)-block-poly (propylene glycol)-block-poly (ethylene glycol) (P123, average $M_n \sim 5800$, AR) and lithium chloride anhydrous (LiCl, 99.99%, AR) were purchased from Shanghai Aladdin Industrial (Shanghai, China). All reagents except styrene were used directly without further purification.

Apparatus and equipment

The equipment was an analytic balance (ME104E), magnetic stirrer (85-2), circulating water vacuum pump (SHZ-IIID), electronic energy-saving thermometer (ZNKW-I), muffle furnace (SX2), vacuum-drying oven (DZF), electro-thermostatic

blast oven (DHG-9070A), gas bath thermostatic oscillator (ZD-85), and PH meter (E-201F).

Preparation of polystyrene hard template

In order to remove the polymerization inhibitor in styrene, styrene monomer and 0.5 M NaOH solution were mixed in a separate funnel with the same volume, and washed repeatedly 4–6 times until the water layer became colorless. Then, the supernatant liquid was washed with ultrapure water until neutral. The synthesis process could be divided into two steps. In the first step, monodispersed PS particles were synthesized by controlling the emulsion polymerization. Then, 0.45 g SDS and 0.6 g $K_2S_2O_8$ were dispersed in a mixture of 150 ml ultrapure water and 270 ml ethanol with magnetic stirring at room temperature to form a homogeneous solution. Under nitrogen atmosphere, 36 ml styrene was injected quickly into the mixture using a syringe. After injection, the temperature was increased to 71 °C and refluxed for 19 h. Finally, the milky product was stored in a clean glass container after the solid material was filtered off. In the second step, the polystyrene emulsion was transferred into a beaker, with a solution height of approximately 1–2 cm. Then, the beaker was placed in a 70 °C oven to evaporate the solvent completely, resulting in a white solid.

Preparation of 3D macroporous–mesoporous lithium titanate

Lithium titanate was prepared based on a previous report [21]. The molar ratio of crude materials was $CH_3COOLi:C_{12}H_{28}O_4Ti:CH_3COOH:i-C_3H_7OH = 4:5:60:100$. Specifically, 1.32 g CH_3COOLi and 0.55 g P123 was added into a mixed solution containing 17.00 mL CH_3COOH and 37.00 mL $i-C_3H_7OH$ with magnetic stirring at room temperature to form a transparent solution. Then, 7.40 mL titanium isopropoxide was dropped into this solution and stirred for 10 min, resulting in a pale yellow solution.

According to the hard template method [22], the prepared lithium titanate precursor was immersed into a PS microarray. After total immersion, vacuum filtration caused the lithium titanate precursor solution to completely fill the cracks of the crystals. Next, PS hard templates were solidified in a 70 °C oven for 24 h by when the solvent had completely evaporated. Finally, the sample was calcined in air at 200 °C for 1 h with a rate of 1 °C/min, then at 600–800 °C for 6 h with a heating ramp of 2 °C/min.

Synthesis of nonporous lithium titanate

Nonporous lithium titanate was synthesized through a sol–gel process followed by calcination treatment [23]. Specifically, 6.70 g $CH_3COOLi \cdot 2H_2O$ was put into 75 mL ethanol and stirred at ambient temperature until the white precipitate dissolved, followed by the addition of 24.28 mL titanium isopropoxide to form a transparent yellow solution, which gradually became a milk-white gel. The resulting gel was placed in a 60 °C vacuum oven for 1 day, and then ground to become a

white powder, which was calcined in air at 800 °C for 12 h under the heating rate of 2 °C/min.

Characterization

X-ray powder diffraction (XRD) was used to examine the crystalline phase of the samples. All samples were detected by an X-ray diffractometer (Rigaku D/MAX-2550). The test conditions were as follows: graphite monochromator, K_{α} radical of Cu (wavelength $\lambda = 0.154$ nm), operating voltage of 40 kV, current of 100 mA, and scan range $2\theta = 5\text{--}80^{\circ}$ with scanning rate of $0.5^{\circ}/\text{min}$. Scanning electron microscopy (SEM) images were conducted by a Japan JSM-6360LV scanning electron microscope with an operating voltage 15 kV. Transmission electron microscopy (TEM) images were obtained from a high-resolution transmission electron microscope with a working voltage of 200 kV. The measurement of the BET (Brunauer–Emmett–Telle) surface area and pore diameter distribution was performed by measuring N_2 adsorption–desorption isotherms at 77 K with a Micrometric ASAP 2020 instrument. An inductively coupled plasma emission spectrum (ICP-OES; Varian 710ES) was utilized to detect ion concentration.

Results and discussion

The influence of calcination temperature and time on the crystalline phase

The influence of the calcination temperature and time on the crystalline phase was investigated by wide-angle XRD analysis. The sample calcined at 600 °C for 3 h shows strong and finely-resolved peaks at $2\theta = 18.33^{\circ}$, 35.57° , 43.24° , 62.83° , ascribed to the reflections of spinel $Li_4Ti_5O_{12}$ with a space group of $Fd\bar{3}m$ (Fig. 1a). The crystal size is calculated to be 11.76 nm according to the Scherrer

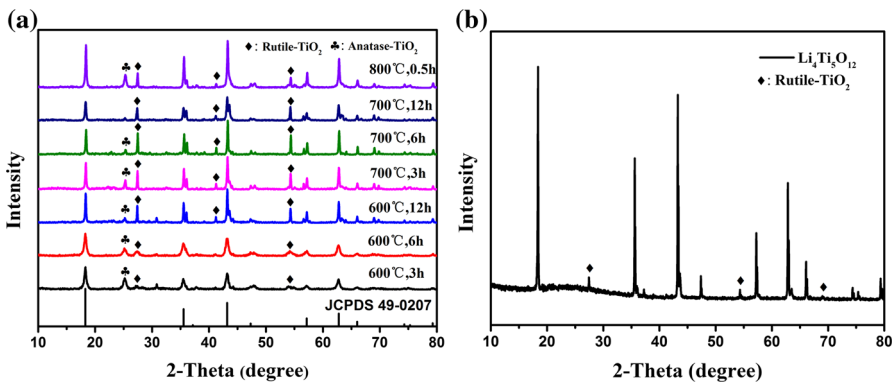


Fig. 1 XRD standard card Standard XRD pattern of $Li_4Ti_5O_{12}$ (JCPDS 49-0207) and XRD patterns of **a** 3DM- $Li_4Ti_5O_{12}$ fabricated under different calcination temperatures by the hard template method; **b** N- $Li_4Ti_5O_{12}$ fabricated by the sol-gel method with the calcination temperature of 800 °C

equation. Meanwhile, weak peaks indexed to anatase ($2\theta = 25.30^\circ$) and rutile ($2\theta = 27.47^\circ, 54.32^\circ$) TiO_2 are also observed. The crystallinity of spinel $\text{Li}_4\text{Ti}_5\text{O}_{12}$ improves with increasing time (6 h, 12 h), and the anatase gradually transforms to rutile TiO_2 . Increasing the temperature to 700°C also produces a mixture composed of mainly spinel $\text{Li}_4\text{Ti}_5\text{O}_{12}$ and tiny amounts of TiO_2 with anatase and rutile phases (3, 6 h). In contrast, the anatase completely turns into rutile phase after 12 h calcination. Further increasing of the calcination temperature to 800°C still does not form a pure spinel $\text{Li}_4\text{Ti}_5\text{O}_{12}$ phase, although the crystallinity becomes much higher after only 0.5 h compared with the product calcined at 700°C for 12 h. Moreover, the XRD pattern of the sample prepared in the absence of the hard template and calcined at 800°C for 12 h also shows a mixture of spinel $\text{Li}_4\text{Ti}_5\text{O}_{12}$ and tiny rutile phases (Fig. 1b). Since the above samples are mainly composed of spinel $\text{Li}_4\text{Ti}_5\text{O}_{12}$, we have called those prepared with and without PS template 3DM- $\text{Li}_4\text{Ti}_5\text{O}_{12}$ and N- $\text{Li}_4\text{Ti}_5\text{O}_{12}$, respectively.

The morphology of $\text{Li}_4\text{Ti}_5\text{O}_{12}$

The SEM image shows that the PS microarray used as the hard template of $\text{Li}_4\text{Ti}_5\text{O}_{12}$ is hexagonally arranged from the PS sphere with a diameter of ca. 330 nm (Fig. 2a). $\text{Li}_4\text{Ti}_5\text{O}_{12}$ obtained through the calcination at 600°C for 6 h has an ordered inverse opal structure as observed from the FESEM image (3DM- $\text{Li}_4\text{Ti}_5\text{O}_{12}$ -600; Fig. 2b). The TEM image clearly shows an interconnected porous structure with a diameter of 165 nm and a wall thickness of 12.5 nm (Fig. 2c), indicating the size contraction of the framework during the calcination treatment. Further increasing the calcination temperature results in the collapse of the macroporous structure (not shown). Figure 2d shows that the sample prepared in the absence of the hard template and calcined at 800°C for 12 h (N- $\text{Li}_4\text{Ti}_5\text{O}_{12}$ -800) is nonporous and highly agglomerated. To understand the effect of the porous structure on the Li^+ adsorption performance, 3DM- $\text{Li}_4\text{Ti}_5\text{O}_{12}$ -600 and N- $\text{Li}_4\text{Ti}_5\text{O}_{12}$ -800 were adopted as the lithium ion sieves in the subsequent study.

Figure 3a demonstrates that the N_2 adsorption–desorption isotherms of 3DM- $\text{Li}_4\text{Ti}_5\text{O}_{12}$ -600 shows a sharp increase in the high relative pressure range of 0.8–1.0, which is characteristic of macroporous structure. Figure 3b obviously presents a significantly decreased N_2 adsorption capacity of N- $\text{Li}_4\text{Ti}_5\text{O}_{12}$ -800 compared with that of 3DM- $\text{Li}_4\text{Ti}_5\text{O}_{12}$ -600. The specific surface area of 3DM- $\text{Li}_4\text{Ti}_5\text{O}_{12}$ -600 is $39.25\text{ m}^2/\text{g}$ calculated from the Brunauer–Emmett–Teller (BET) method, which is much larger than that of N- $\text{Li}_4\text{Ti}_5\text{O}_{12}$ -800 ($1.24\text{ m}^2/\text{g}$). A weak pore-size distribution curve with the mean value of $\sim 20\text{ nm}$ is obtained from the adsorption branch of N- $\text{Li}_4\text{Ti}_5\text{O}_{12}$ -800 using the BJH (Barrett–Joyner–Halenda) model. In comparison, a strong pore-size distribution curve with a mean value of $\sim 25\text{ nm}$ is obtained from the adsorption branch of 3DM- $\text{Li}_4\text{Ti}_5\text{O}_{12}$ -600, demonstrating the existence of abundant interstitial mesopores in the framework due to the crystallite stacking.

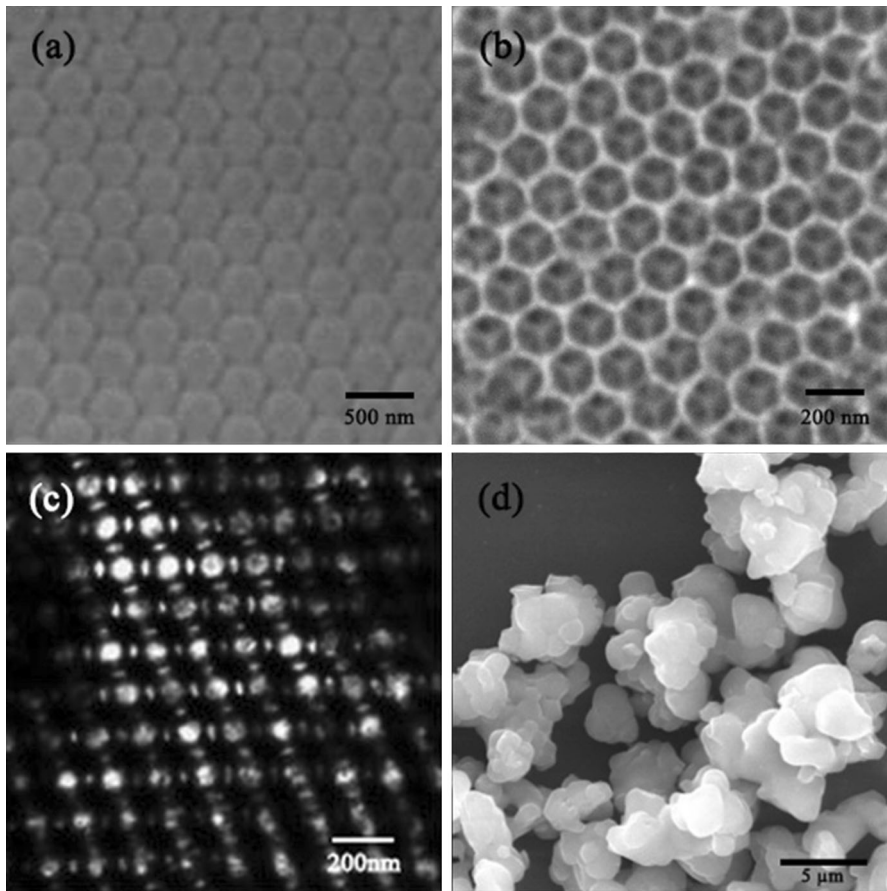


Fig. 2 **a** SEM image of PS colloidal crystal template arrays; **b, c** FESEM and TEM images of 3DM- $\text{Li}_4\text{Ti}_5\text{O}_{12}$ -600 with the calcination temperature of 600 °C for 6 h. **d** SEM image of nonporous N- $\text{Li}_4\text{Ti}_5\text{O}_{12}$ fabricated by the sol–gel method with the calcination temperature of 800 °C

Acid extraction of $\text{Li}_4\text{Ti}_5\text{O}_{12}$

$\text{Li}_4\text{Ti}_5\text{O}_{12}$ was acid-washed with HCl to extract Li^+ , where the dissolution rates of Li^+ (α_{Li}) and Ti^{4+} (β_{Ti}) were used to measure the extraction efficiency and the stability of the lithium ion sieve, respectively. Equation (1) has been used to calculate α_{Li} and β_{Ti} ,

$$\alpha_{\text{Li}}(\text{or } \beta_{\text{Ti}}) = CV/S \quad (1)$$

where C (g/L) is the concentration of Li^+ (or Ti^{4+}) in the acid solution, V (L) is the volume of the solution, and S (g) is the mass of lithium or titanium in the lithium ion sieve.

The Li^+ adsorption capacity is calculated using Eq. (2),

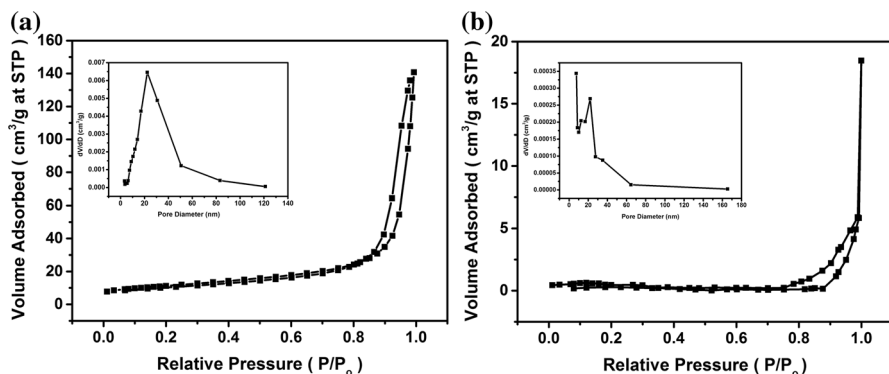


Fig. 3 Nitrogen adsorption/desorption isotherms of **a** 3DM-Li₄Ti₅O₁₂-600 and **b** N-Li₄Ti₅O₁₂-800. Inset the corresponding pore-size distribution curve

$$Q = (C_0 - C_t) V/m \quad (2)$$

where C_0 (mmol/L) is the initial concentration of Li⁺, C_t (mmol/L) is the concentration of Li⁺ at different times, V (L) is the solution volume and m (g) is the weight of the lithium ion sieve.

The influence of HCl concentration (C_{HCl}) and acid treatment time on the extraction performance for lithium ions was investigated at room temperature by dispersing 0.2 g N-Li₄Ti₅O₁₂-800 into 20 ml HCl solution with different concentrations (0.05, 0.1, 0.5, 1.0 and 5.0 M) at 25 °C. The supernatant liquid was analyzed by ICP-OES after different times (24, 48, 72 and 96 h). As shown in Fig. 4a, the dissolution rate of lithium ion slightly increases from 13 to 15% after 24 h when C_{HCl} increases from 0.05 to 0.1 M, while the titanium ion shows no loss (Fig. 4b). The lithium extraction rate does not show any further increase until C_{HCl} abruptly reaches 5.0 M (ca. 31%). Unfortunately, Ti⁴⁺ begins to dissolve when C_{HCl} is over 0.1 M, and the rate increases to 10% at $C_{\text{HCl}} = 5.0$ M. Meanwhile, the

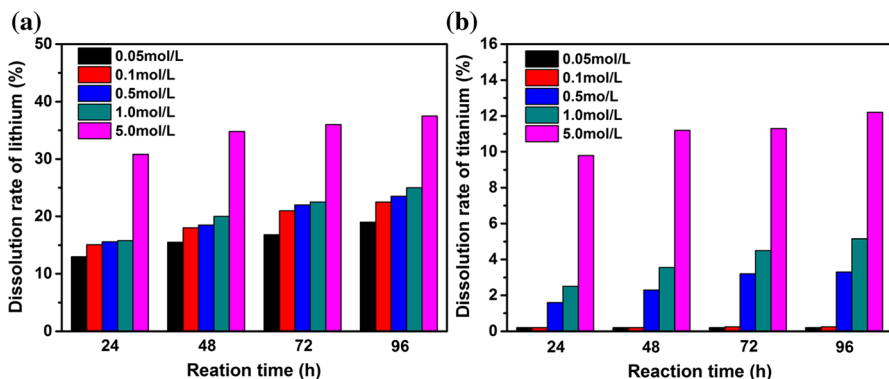


Fig. 4 Extraction of Li⁺ from N-Li₄Ti₅O₁₂-800 in the presence of hydrochloric acid with different concentrations: **a** dissolution rate of Li⁺, **b** dissolution rate of Ti⁴⁺

prolonging of the acid treatment time from 24 to 96 h causes the gradual growth of the lithium dissolution rate in a wide C_{HCl} range from 0.05 to 5.0 M, although the growth percentage slows down during the washing time. In contrast, the loss rate of Ti^{4+} stays negligible even after 96 h when C_{HCl} ranges from 0.05 to 0.1 M, which then rises steadily at a higher C_{HCl} .

Based on the above results, C_{HCl} was then fixed at 0.1 M in the subsequent study to maximize the extraction ratio of Li/Ti. The acid washing time was further prolonged to achieve more extraction of Li^+ . As shown in Fig. 5, only ca. 53% of Li can be extracted even after 15 days washing at room temperature. In contrast, the dissolution rate is over 50% after 7 days (not shown) when the washing temperature increases to 80 °C and finally reaches ca. 93% after 15 days, indicating that the higher temperature can greatly accelerate the extraction of lithium ions. 3DM- $\text{Li}_4\text{Ti}_5\text{O}_{12}$ -600 was then acid-washed with 0.1 M of HCl solution at 80 °C. Almost 100% lithium was extracted after only 72 h, suggesting the macroporous–mesoporous structure is extremely beneficial to improving the accessibility of H^+ to Li^+ in $\text{Li}_4\text{Ti}_5\text{O}_{12}$ and the subsequent diffusion of Li^+ into the solution.

The phase transformation after lithium extraction is further characterized by wide-angle XRD patterns (Fig. 6a), where the characteristic diffraction peaks of 3DM- $\text{Li}_4\text{Ti}_5\text{O}_{12}$ -600 disappear after washing at 80 °C for 72 h, further verifying the complete removal of lithium from 3DM- $\text{Li}_4\text{Ti}_5\text{O}_{12}$ -600 and the formation of the 3DM- $\text{H}_4\text{Ti}_5\text{O}_{12}$ -600 lithium ion sieve with lithium ion vacancies. In contrast, the diffraction peaks attributed to the spinel phase in N- $\text{Li}_4\text{Ti}_5\text{O}_{12}$ -800 do not show a prominent intensity decrease until after 7 days (Fig. 6b).

The adsorption performance for Li^+ was carried out by dispersing 0.1 g 3DM- $\text{H}_4\text{Ti}_5\text{O}_{12}$ -600 from 3 days washing or N- $\text{H}_4\text{Ti}_5\text{O}_{12}$ -800 from 15 days washing at 80 °C into 20 ml 0.05 M LiOH solution, which was thermostatically oscillated for 24 h. The ICP-OES test results in Fig. 7 show that the saturated adsorption capacities of the 3DM- $\text{H}_4\text{Ti}_5\text{O}_{12}$ -600 lithium ion sieve reaches 5.51 mmol/g

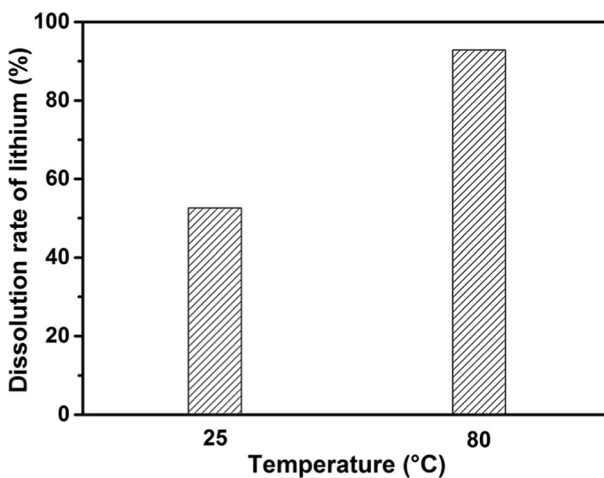


Fig. 5 Extraction of Li^+ from N- $\text{Li}_4\text{Ti}_5\text{O}_{12}$ -800 at different temperatures; concentration of HCl: 0.1 M

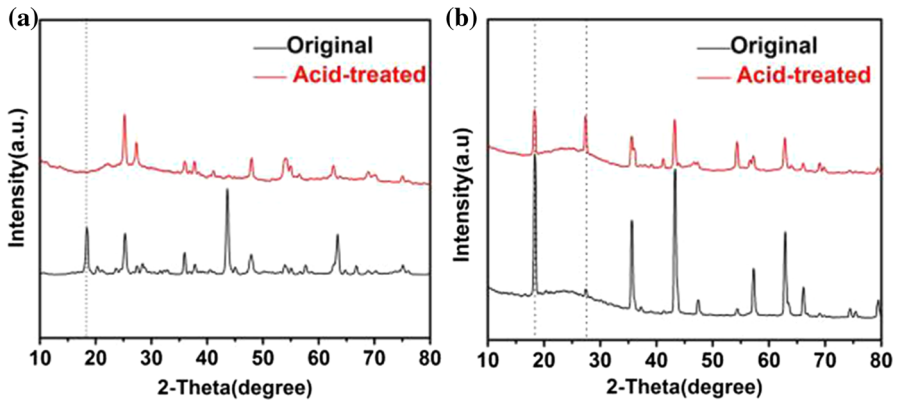


Fig. 6 XRD patterns of **a** 3DM-Li₄Ti₅O₁₂-600, **b** N-Li₄Ti₅O₁₂-800 before (lower line) and after (upper line) the acid treatment. Reaction time: **a** 72 h, **b** 7 days; concentration of HCl: 0.1 M

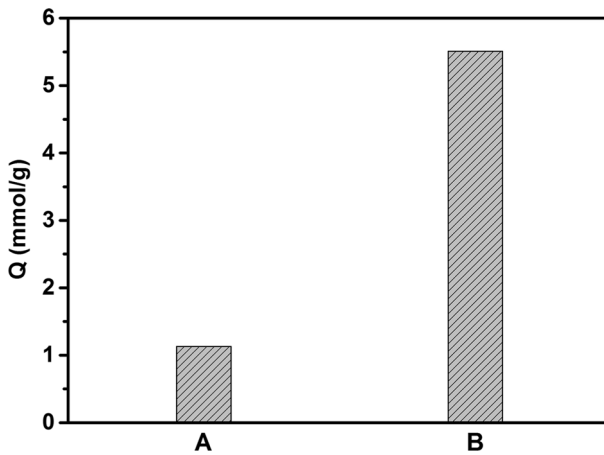


Fig. 7 The saturation adsorption capacity of *a* N-H₄Ti₅O₁₂-800 and *b* 3DM-H₄Ti₅O₁₂-600. Reaction time: 24 h; initial concentration of LiOH: 0.05 M

(Eq. 2), much higher than that of the nonporous lithium ion sieve, N-H₄Ti₅O₁₂-800 (1.12 mmol/g). The improved adsorption rate for Li⁺ of 3DM-H₄Ti₅O₁₂-600 should be attributed to its macroporous-mesoporous structure, providing very open and accessible vacancies for Li⁺.

Selectivity and recyclability of 3DM-H₄Ti₅O₁₂-600 lithium ion sieve

The selectivity of 3DM-H₄Ti₅O₁₂-600 towards Li⁺ has been further studied based on Eqs. (3) and (4) using different metal ions (Na⁺, K⁺, Mg²⁺ and Ca²⁺) as competitive ions, where K_d , α_{Me}^{Li} and C_e refer to the distribution coefficient, separation factor and equilibrium concentration [24].

Table 1 Performance of separating Li^+ from other cations by 3DM- $\text{H}_4\text{Ti}_5\text{O}_{12}$ -600

| Cations | C_0 (mmol/L) | C_e (mmol/L) | Q (mmol/g) | K_d (ml/g) | $\alpha_{\text{Me}}^{\text{Li}}$ |
|------------------|----------------|----------------|--------------|--------------|----------------------------------|
| Li^+ | 8.78 | 7.13 | 0.22 | 30 | 1.00 |
| Na^+ | 11.08 | 10.55 | 0.07 | 7 | 4.29 |
| K^+ | 11.33 | 11.04 | 0.04 | 4 | 7.50 |
| Ca^{2+} | 10.94 | 10.39 | 0.07 | 7 | 4.29 |
| Mg^{2+} | 10.15 | 10.05 | 0.01 | 1 | 30.00 |

$$K_d = (C_0 - C_e)V/(C_e m) \quad (3)$$

$$\alpha_{\text{Me}}^{\text{Li}} = K_{d,\text{Li}}/K_{d,\text{Me}} \quad \text{Me: Li, Na, K, Mg, Ca.} \quad (4)$$

The distribution coefficient (K_d , Eq. 3) is the parameter related to the adsorption capacity (Q), and the separation factor $\alpha_{\text{Me}}^{\text{Li}}$ (Eq. 4) is used to measure the separation degree of Li^+ from other metal ions. In general, a higher distribution coefficient means that the lithium ion sieve has a larger adsorption capacity for the target substance. Meanwhile, the higher separation factor is also proof of the higher selectivity of the lithium ion sieve to lithium ions.

The selectivity of the lithium ion sieve was explored by dispersing the 3DM- $\text{H}_4\text{Ti}_5\text{O}_{12}$ -600 lithium ion sieve into $\text{NH}_3\cdot\text{H}_2\text{O}$ - NH_4Cl buffer solution (0.01 M) containing mixed ions of Li^+ , Na^+ , K^+ , Mg^{2+} and Ca^{2+} (pH = 10.92). The concentration of metal ions in the supernatant was measured by ICP-OES after the adsorption equilibrium. Table 1 implies that the lithium ion sieve has a greater adsorption capacity towards Li^+ (0.22 mmol/g) compared with other ions (< 0.1 mmol/g). The distribution coefficient of the lithium ion sieve to Li^+ is 30 ml/g, much larger than that of the other cations (1–7 ml/g). The separation factor

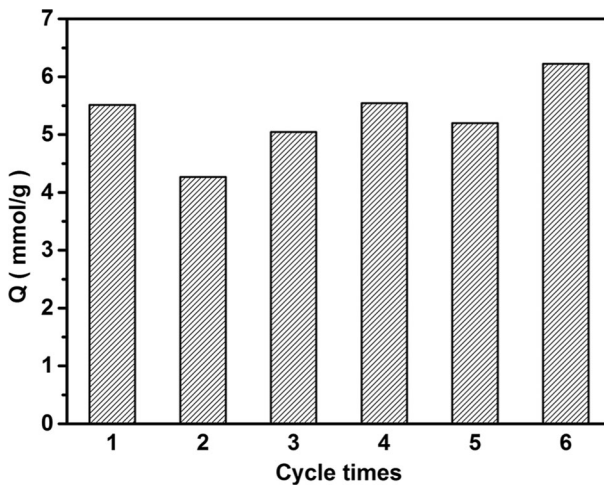


Fig. 8 The recycle performance of 3DM- $\text{H}_4\text{Ti}_5\text{O}_{12}$ -600. Reaction time: 72 h (acid washing), 24 h (lithium adsorption), C_{HCl} : 0.1 M, C_{LiOH} : 0.05 M

of the lithium ion sieve to other metal ions follows the order: $\text{Li}^+ < \text{Na}^+ \sim \text{Ca}^{2+} < \text{K}^+ < \text{Mg}^{2+}$.

The recyclability of the 3DM- $\text{H}_4\text{Ti}_5\text{O}_{12}$ -600 lithium ion sieve was studied by dispersing 0.1 g 3DM- $\text{Li}_4\text{Ti}_5\text{O}_{12}$ -600 into 20 ml 0.1 M HCl solution at 80 °C for 72 h. The product was washed with water until it became neutral and then dried in a 70 °C oven. The regenerated sample was then re-treated with LiOH solution (20 ml, 0.05 M). The supernatant liquid was diluted and analyzed by ICP-OES after 24 h. Figure 8 shows that the saturated adsorption capacity varied within 20% during 6 cycles, demonstrating the good recyclability of the 3DM- $\text{H}_4\text{Ti}_5\text{O}_{12}$ -600 lithium ion sieve.

Conclusions

3DM- $\text{Li}_4\text{Ti}_5\text{O}_{12}$ prepared via the hard-template method was transformed into 3DM- $\text{H}_4\text{Ti}_5\text{O}_{12}$ after acid leaching. The 3D macroporous structure significantly accelerated the deintercalation and intercalation of Li^+ from and into the vacancies in the framework. The saturated adsorption capacity of 3DM- $\text{H}_4\text{Ti}_5\text{O}_{12}$ reached 5.51 mmol/g, much higher than that of its nonporous counterpart (1.12 mmol/g). The high distribution coefficient and separation factor towards Li^+ were verified using Na^+ , K^+ , Mg^{2+} and Ca^{2+} as competitive ions, demonstrating the excellent Li^+ selectivity of 3DM- $\text{H}_4\text{Ti}_5\text{O}_{12}$.

Acknowledgements This work is supported by the National Natural Science Foundation of China (21673073, 21677048, U1407102 and 21377038), the National Basic Research Program of China (973 Program, 2013CB632403), the Science and Technology Commission of Shanghai Municipality (14230710500, 14ZR1410700 and 16JC1401400) and the Fundamental Research Funds for the Central Universities, PetroChina Innovation Foundation (2015D-5006-0402), the Fundamental Research Funds for the Central Universities (222201717003) and Collaborative Innovation Fund of Shanghai Institute of Technology (XTCX2015-9).

References

1. K. Qian, L.K. Tang, M. Wagemaker, Y.B. He, D.Q. Liu, H. Li, R.Y. Shi, B.H. Li, F.Y. Kang, *Adv. Sci.* **1700205**, 7 (2017)
2. L. Wang, W. Ma, M. Han, C.G. Meng, *Acta Chim. Sin. Chin. Ed.* **65**, 1135 (2007)
3. S.A. Hong, A. Nugroho, S.J. Kim, J. Kim, K.Y. Chung, B.W. Kang, *Res. Chem. Intermed.* **429**, 37 (2011)
4. D.Z. Lin, *China Saf. Sci. J.* **72**, 14 (2004)
5. Y. Guo, Y.L. Ying, Y.Y. Mao, X.S. Peng, B.L. Chen, *Angew. Chem. Int. Ed.* **15120**, 55 (2016)
6. S.Y. Sun, F. Ye, X.F. Song, Y.Z. Li, J. Wang, J.G. Yu, *Chin. J. Inorg. Chem.* **439**, 27 (2011)
7. J.M. Nan, D.M. Han, X.X. Zuo, *J. Power Sources* **278**, 152 (2005)
8. H.B. Li, L.D. Zou, *Desalination* **62**, 275 (2011)
9. J.W. An, D.J. Kang, K.T. Tran, M.J. Kim, *Hydrometallurgy* **64**, 117 (2012)
10. X.H. Li, C.J. Zhang, S.N. Zhang, J.X. Li, *Desalination* **26**, 369 (2015)
11. X.Y. Guo, X. Cao, G.Y. Huang, Q.H. Tian, H.Y. Sun, *J. Environ. Manag.* **84**, 198 (2017)
12. Q.H. Zhang, S.P. Li, S.Y. Sun, X.S. Yin, J.G. Yu, *Chem. Eng. Sci.* **169**, 65 (2010)
13. Y.E. Zhang, H. Wang, B. Wang, *Res. Bull.* **1411**, 37 (2002)
14. C. Özgür, *Solid State Ionics* **1425**, 181 (2010)
15. J.L. Xiao, S.Y. Sun, P. Li, *Ind. Eng. Chem. Res.* **11967**, 52 (2013)

16. K. Hideki, M. Osamu, K. Yoshio, J. Electroanal. Chem. **77**, 559 (2003)
17. D.Q. Dong, F.B. Zhang, G.L., Zhang. Acta Phys. Chim. Sin. **950**, 23 (2007)
18. L.W. Ma, B.Z. Chen, Y. Chen, X.C. Shi, Microporous Mesoporous Mater. **147**, 142 (2011)
19. Q.H. Zhang, S.P. Li, S.Y. Sun, Chem. Eng. Sci. **165**, 65 (2010)
20. X. Xu, Y.M. Chen, P.Y. Wan, K. Gasem, K.Y. Wang, T. He, H. Adidharma, M.H. Fan, Prog. Mater Sci. **276**, 84 (2016)
21. S.W. Woo, K. Dokko, K. Kanamura, Electrochim. Acta **79**, 53 (2007)
22. D.Y. Qi, L.J. Lu, L.Z. Wang, J.L. Zhang, J. Am. Chem. Soc. **9886**, 136 (2014)
23. S. Bach, J.P. Pereira-Ramos, N. Baffier, J. Powder Sources **273**, 81 (1999)
24. L.A. Limjuco, G.M. Nisola, C.P. Lawagon, S.P. Lee, J.G. Seo, H. Kim, W.J. Chung, Colloids Surf. A **267**, 504 (2016)